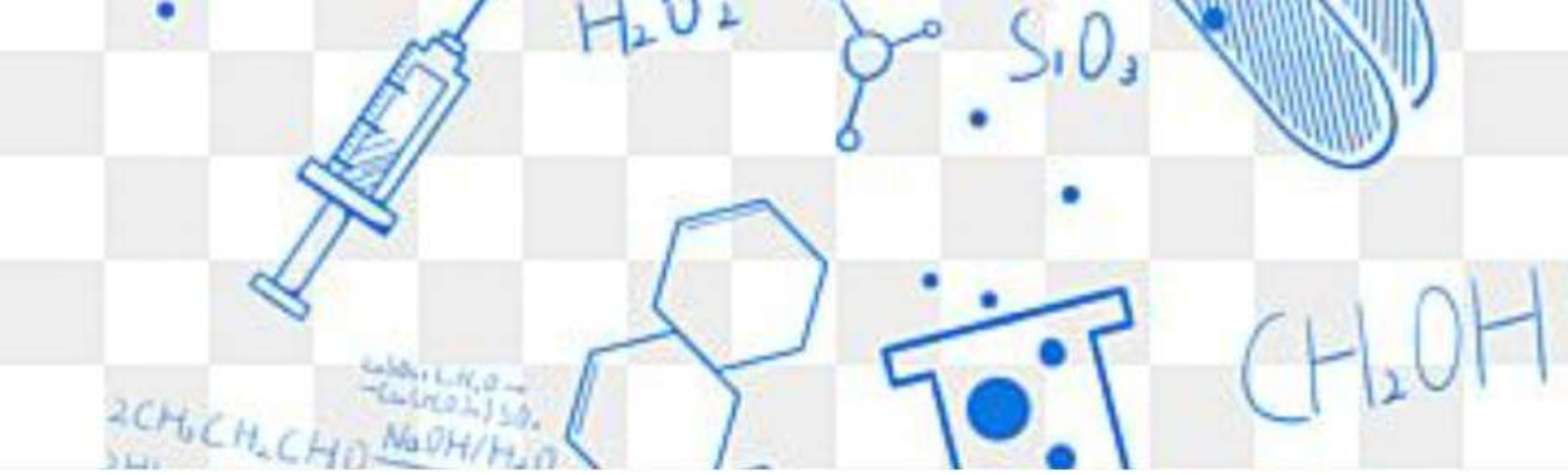

Journal of the Korean Ceramic Society
Vol. 54, No. 2, pp. 158~166, 2017.

https://doi.org/10.4191/kcers.2017.54.2.11

Enhanced Hemolytic Biocompatibility of Hydroxyapatite by Chromium (Cr^{3+}) Doping in Hydroxyapatite Nanoparticles Synthesized by Solution Combustion Method

Sneha S. Bandgar*, Tanaji V. Kolekar*******‡,**

ABSTRACT

For the better success of biomedical implant surgery, we used a modified solution combustion method to synthesize Hydroxyapatite (HA) and Chromium (Cr^{3+}) modified Cr-HA with different concentrations of 0.5, 1.0, 1.5, 2.0 and 2.5. The Cr-HA nanopowder was characterized by TGA, XRD, SEM-EDS and TEM. The HA and Cr-HA powders were subjected to *in vitro* biological studies to determine their biocompatibility and hemocompatibility. The cytotoxicity of HA and Cr-HA were evaluated on Hela (Cervical cancer) cells and L929 (mouse fibroblast) cells by using MTT assay. Hemocompatibility studies demonstrated a noticeable haemolytic ratio below 5%, which confirms that these materials are compatible in nature with human blood. The results of the present work confirm that the synthesised HA and Cr-HA are biocompatible and can be extensively used in the biomedical field to improve overall material biological properties.

Key words : Cr-Hydroxyapatite, MTT assay, Hela(Cervical cancer) and L929 cells, Hemolysis, Biomedical applications

1. Introduction

Recently, materials science research has come to involve applications of materials to biomedical engineering, especially in orthopaedic implant surgery. Certain metal oxide and ceramic materials have been used in the biomedical field for more than four decades to repair and reconstruct diseased orthopedic parts.[1] Bio-inert ceramics are special types of nanocrystalline bioceramic materials that are used for the repair and reconstruction of damaged or diseased parts of the body. It is reported that the first well-known bioceramic material was calcium sulphate (plaster of Paris).[2] Among the different ceramic materials, calcium phosphate based bio ceramic nanoparticles, owing to their biocompatibility behaviour, are promising candidates for biomedical applications, such as a drug delivery, detection of pathogens, and enzyme immobilization. One of the most interesting and attractive bioceramic materials, Hydroxyapatite (HA), has been studied in tissue engineering for orthopedics and dentistry due to its bioactivity, biocompatibility and osteoconductivity. The structural and chemical composition of HA is similar to the mineral components of mammalian bone and teeth.[3-5] Improvement in the biocompatibility and nontoxicity of bone substitute materials is one of the main concerns of orthopedic and dental surgery. Since the 1980s, Hydroxyapatite has been widely used as a coating on metallic implants to improve their biocompatibility.[6-8]

To use in implants of artificial bone, ceramic material should be resorbable, easy to shape, and possess osteoinductive mechanical properties. Nowadays, the most frequently used calcium phosphate based compound is hydroxyapatite, processed as porous ceramics, coatings, and composites Artificial HA is a good candidate and is widely applicable in the field of biomedical engineering.[9,10] The function of a bioceramic is not only physical substitution but also participation in the bone regeneration process of the artificial component(s). HA, because of its good biocompatibility, has been found to be applicable as a biomaterial in orthopedics, bioengineering, and dentistry.[11] Some of the most promising characteristics of Synthetic HA are its very good ion (cation) exchange rate with metals, its high affinity for pathogenic microorganisms, and its excellent biocompatibility.[12-14] It is reported that around 70 - 80% of implants are made of biocompatible metals.[15] With the introduction of a transition metal ion like silver, HA can be effective in controlling microorganisms due to its ion-exchange capabilities.[16]

†Corresponding author : Sambhaji R. Bamane
E-mail : sambhajibamane@yahoo.com
Tel : +91-2161-262475 Fax : +91-2161-26222324
‡Corresponding author : Tanaji V. Kolekar
E-mail : rhts.kolekar@gmail.com
Tel : +91-2342-220328 Fax : +91-2342-220989

Metal doping in HA for biomedical applications has received a lot of attention because it is capable of enhancing the biocompatibility response by lowering the toxicity of the nanoparticles. It is well known that metal ion doping in HA can influence the biological properties of metal-doped HA by improving the overall antimicrobial and non-cytotoxicity. Free radicals are produced in oxidation reactions. These free radicals initiate chain reactions, which interact with and damage cells. To terminate these reactions, antioxidants play an important role by leaving free radical intermediates, and stop other oxidation reactions. It has been reported that Ca sites by some trivalent (Al^{3+}, Fe^{3+}) and divalent cations (Ba^{2+}, Mg^{2+}, Sr^{2+}, Cd^{2+}).[17] This is a major drawback when a bio-ceramic material is implanted in a body; the material can release harmful metal ions due to wear and corrosion . Out of metal ion release, some toxic metal ions can have bad effects on the surrounding environment.[18]

Most of the biological properties of ceramic materials depend on the size and shape of the ceramic nanoparticles, which characteristics are closely related to the synthesis method. It is reported that patients who undergo metal-on-metal resurfacing have raised serum levels of Cr ions (0.8 μg l$^{?}$1).[19] Chromium metal has different states of oxidation, which is a useful component of metalloproteins and enzymes.[20] In prosthesis surgery, antibiotic therapy is used to avoid bacterial infections in artificial bones. If in any case post-surgery infection spreads, it may necessitate the removal of the prosthetic part. Similarly, it is used in orthopedic surgery and stomatology. The success of any implant surgery depends on the antibacterial properties and nontoxic nature of the surroundings. Due to secondary bacterial infections, it causes serious complications. Trivalent Cr(III) and hexavalent Cr(VI) are the two most common oxidative states of Cr. Hexavalent Cr(VI) is toxic in nature. Chromium is an environmentally hazardous material and is carcinogenic.[21] It is reported that Cr^{3+} ions have been studied in few studies to verify their effectiveness in encouraging a biological response; also, this ion affects the crystallisation behaviour of hydroxyapatite bio ceramics and bone minerals.[22] *In vitro* study of Cr(VI) with red blood cells for 40 min shows no effect at up to 1 g/l.[23] It has been reported that Cr(III) dopant improves the photo catalytic antibacterial activity under visible light irradiation.[24]

The aim of the present study was to investigate the role of chromium ions at different concentrations on *in vitro* L929 cell lines and Hela cervical cell lines for 24 h and 48 h. Chromium modified Hydroxyapatite was prepared by facial solution combustion method. This work's focus was to study the bioactivity of Cr-HA nanoparticles under different physical and biological conditions. The prepared Cr substituted HA was characterized by TGA, Powder-XRD, SEM-EDAX, HR-TEM, and XPS. It has been reported that nanoparticles may produce toxicity in some cell-based assays, but not in all. This toxicity is a result of differences in the inborn response of particular cell types, which cause interference with chemical probes; therefore, it is suggested that the *in vitro* cytotoxicity activities of HA should be assessed for several cell types with different assays and doses, in order to evaluate the cytotoxicity of Cr doped HA for study.

2. Experimental Procedure

2.1. Materials

Chromium nitrate (III) was purchased from Thomas Baker. Calcium nitrate tetrahydrate ($Ca(NO_3)_2{\cdot}4H_2O$), and *di*-Ammonium hydrogen orthophosphate ($(NH_4)_2HPO_4$ were purchased from Sigma-Aldrich. All chemicals were used without any purification and all were analytical grade.

2.2. Synthesis of Pure HA and Cr-doped hydroxyapatite

Cr modified hydroxyapatite (Cr-HA) was prepared by a modified solution combustion method with different concentrations (0.0, 0.5, 1.0, 1.5, 2.0, 2.5 mole %). Stoichiometric amounts of the calcium precursor $Ca(NO_3)_2{\cdot}4H_2O$, Chromium nitrate (III), and phosphate precursor $(NH_4)_2HPO_4$ were dissolved in double distilled water to obtain a final concentration of solution of 0.1 M. Polyvinyl alcohol (PVA) was used as a fuel. In double distilled water, an equimolar solution of PVA was prepared. The equimolar mixture of fuel and oxidants was stirred magnetically for 30 min at room temperature. After evaporation, this mixture formed a gel of precursors at 100°C; then, this gel was heated at 300°C to obtain a black colored powder. The obtained powder of Cr-HA was then annealed at 950°C for 6 h. Using a muffle furnace, it was possible to ignite the dried mixture to start the combustion reaction. Various Cr-doped hydroxyapatite samples containing Cr contents of 0.0, 0.5, 1.0, 1.5, 2.0, and 2.5 mole % were denoted as HA, Cr-HA-1, Cr-HA-2, Cr-HA-3, Cr-HA-4, and Cr-HA-5, respectively.

2.3. Characterization

2.3.1. Structural and morphological studies

The synthesized samples were characterized by various techniques such as TGA, XRD, SEM, Energy Dispersive Spectroscopy (EDS), and TEM. Structural analysis of Cr-HA was performed using X-ray diffraction (Philip-3710) with Cu-Kα radiation. X-ray diffraction patterns were analyzed using the X-pert high score plus software program and obtained XRD patterns were then compared with standards established by the Joint Committee on Powder Diffraction and Standards (JCDPS), to obtain the correct phase structure. Thermo gravimetric analysis (TGA) was used for thermal analysis; in this analysis, changes in the chemical and physical properties of the materials are measured with constant heating rate as a function of increasing temperature. Particle size and morphology were observed using a transmission electron microscope (TEM, JEOL-JEM-2100) with resolution of 2.4 Å. The elemental analysis was carried out by energy dispersive spectroscopy (EDS, JEOL JSM 6360).

2.4. Cytotoxicity study

2.4.1. Cell culture

Comparative *in vitro* Cytotoxicity analysis of the Cr-HA nanoparticles was carried out on Hela (Cervical cancer) cells and L929 (mouse fibroblast) cells using MTT assay. Cell lines were obtained from the National Centre for Cell Sciences, Pune (India). *In vitro* cytoxicity study was carried out at the National Toxicology Centre, Pune (ISO10993/USP 32 NF 27). Target cell lines were grown in MEM culture medium with antibiotics and 10% FBS [foetal bovine serum, kanamycin (0.1 mg/mL^{-1})], penicillin-G (100 U/mL^{-1}), and sodium bicarbonate (1.5 mg/mL^{-1}) at 37°C in a 5% CO_2 atmosphere.

2.4.2. MTT assay

The Hela (Cervical cancer) cells and L929 (mouse fibroblast) cells were separately incubated with concentrations of 1×10^5 cells/ml in medium in a 96-well microtiter plate (cell count was taken in Neubauer's chamber) for 24 h and 48 h. After 24 h fresh media was replaced by the old media and by different proportions of Cr-HA particles of 10, 50, 100, 200, 400, and 800 µg/ml of cultured media. Then, the total medium was incubated at 37°C in a 5% CO_2 atmosphere for 24 h. After 24 h, to confirm the non-contamination and to verify certain other parameters, incubation plates were observed under an inverted microscope. Then, 10 µl of 5 mg/ml MTT solution was added to each well including the control wells. The plates were wrapped in aluminium foil and incubated for 4 h at 37°C in a 5% CO_2 atmosphere for metabolization of MTT with the nanoparticles and cell media. After 4 h of incubation, the plates were removed and observed under an inverted microscope and photographs were taken. The entire medium was then removed by flicking the plates and only the anchored cells remained in the wells. Then, the cells were washed with phosphate buffer saline (PBS) and the formazan that had formed was extracted in 200 µl acidic isopropanol in each well; after 1 h, the absorbance was measured at 492 nm, and from these absorbance values the cell viability was calculated. The experiments were replicated three times and the mean data were graphically presented as mean ± SD. Obtained relative cell viability values (%) compared with control well containing cells without nanoparticles were calculated by the following equation:

$$\text{Relative cell viability (\%)} = [A_{absorbance}]_{tested} / [A_{absorbance}]_{control} \times 100 \quad (1)$$

2.5. In vitro Hemocompatibility

To prove that HA and Cr-HA are good blood biocompatible materials, a comparative Hemolysis test (*in vitro* hemocompatibility) study was carried out for the undoped HA and Cr-HA.

In this Hemolysis test, 5 ml of blood was collected from a healthy volunteer. The healthy volunteer was from our laboratory research group and the person's age was 28 years. In the hemolytic test, it is essential to separate the plasma from the red blood cells; for this reason, the obtained total blood (5 ml) was continuously centrifuged for 4 min at 5000 rpm to separate the plasma from the RBC pellets. After completion of the centrifugation, the plasma separated RBC pellet was diluted with 5 ml of freshly prepared phosphate buffer saline (PBS) solution and this mixture was centrifuged at 4°C for 6 min at 5000 rpm. This centrifugation process was repeated for 6 min with 5 ml of PBS solution; then, the blood pellet was dissolved in 15 ml of phosphate buffer saline (PBS) solution and stored in a refrigerator. Then, the prepared blood sample (0.2 ml) was mixed with 0.8 ml of phosphate buffer saline (PBS) solution containing pure HA and different concentrations of Cr-HA of 0.0, 0.5, 1.0, 1.5, 2.0, and 2.5 and samples were incubated for 1 h at 37°C. After the 1 h incubation period, all tubes were centrifuged at 5000 rpm for 6 min and the obtained supernatant solution was carefully collected and transferred to a 96 well cell culture plate for spectroscopic analysis. The optical density (OD) was measured by BIORAD 680 at 570 nm. Similarly, a phosphate buffer saline (PBS) solution was used as a negative control and deionized water was used as a positive control by mixing both of these liquids with 0.2 ml of blood.

The degree of Hemolysis of pure HA and Cr-HA was calculated by the following equation.

$$\text{Hemolyss(\%)} = \frac{\text{O.D. of sample} - \text{O.D. of negative control}}{\text{O.D. of positive control} - \text{O.D. of negative control}} \times 100 \quad (2)$$

3. Results and Discussion

3.1. Thermogravimetric analysis

Thermogravimetric analysis (TGA) curves of pure HA and of the representative Cr-HA-5 are depicted in Fig. 1. A total of five different stages were observed during the total weight loss. Between room temperature and 250°C, the first

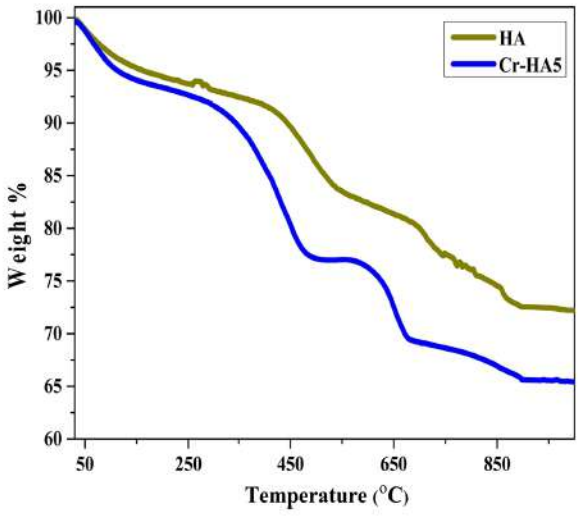

Fig. 1. TGA pattern of pure HA and Cr-HA-5 nanoparticles.

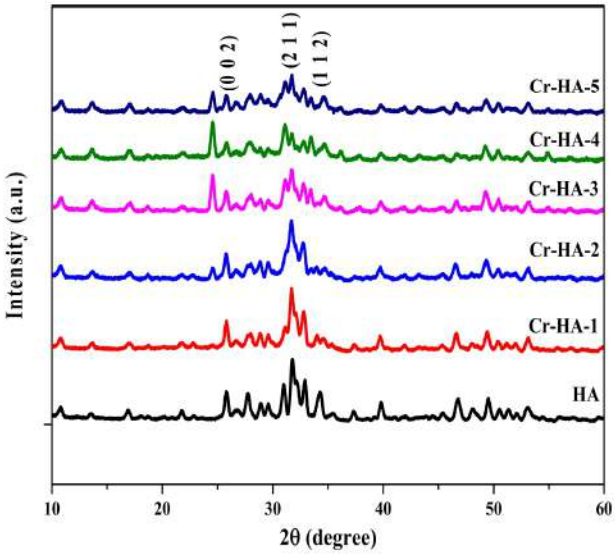

Fig. 2. XRD patterns of pure HA and Cr-HA nanoparticles.

stage of weight loss was observed to take place due to the loss of physically adsorbed water. Due to the loss of organic groups, chemisorbed water and attached solvent to the sample, the second stage of weight loss was found to occur from 250 to 450°C; this was followed by the third stage of weight loss from 450 to 650°C. The fourth stage of weight loss from 650 to 870°C corresponds to the decomposition of carbonate into CO_2. The fifth stage from 870°C onwards shows weight loss less than 0.65%. Therefore, for further characterization and studies, all Cr-HA samples are calcinated at 900°C.

3.2. XRD analysis

Figure 2 shows the purity and phase formation at 900°C for 2 h heat treated HA and Cr-HA.

The XRD of pure HA shows characteristic diffraction peaks that are matched with the standard pattern of HA (JCPDS card number: 09-432) and that confirm the crystalline phase formation. The XRD patterns of Cr-HA with 0.5, 1.0, 1.5, 2.0, and 2.5 concentrations are shown in Fig. 2. The

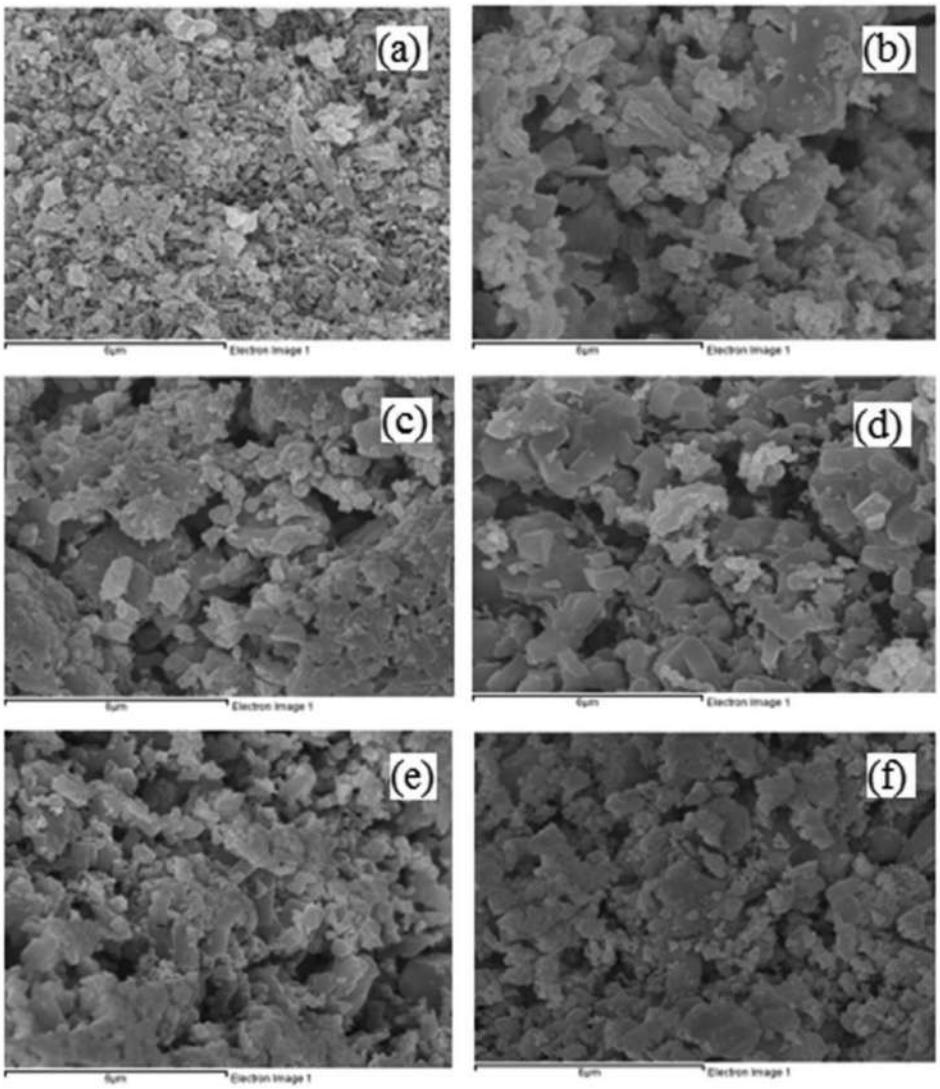

Fig. 3. SEM images of (a) pure HA, (b) Cr-HA-1, (c) Cr-HA-2, (d) Cr-HA-3, (e) Cr-HA-4, and (f) Cr-HA-5.

formation of pure phase Cr doped HA without any other secondary phases and matching all the diffraction peaks were observed. Peak intensity and broadness were found to decrease with an increase in the addition of Cr^{3+} concentration in the HA crystal structure.

The crystallinity and size of the crystallites were found to decrease from 0.5 to 2.5% due to the integration of Cr^{3+} ions into the HA lattice. In the HA lattice it was observed that there was a slight change in the lattice parameter values, i.e. the "a" and "c" axes increased in the Cr^{3+} ion dopant, which indicates the slight replacement of Ca^{2+} with Cr^{3+} ion. The Debye Scherrer equation was used to calculate the crystallite size (D) from the Gaussian fit of the most intense peak (211).

$$D = \frac{0.9\lambda}{\beta\cos\theta} \tag{3}$$

where λ is the wavelength of Cu-Kα radiation (λ = 1.5405 Å), β is the full width at half maxima of the most intense peak (211), θ is the corresponding Braggs diffraction angle, and D is the crystallite size. The average crystallite sizes of HA and Cr-HA were found to be 28.50 nm and 22.12 nm, respectively. The reflection peaks are quite broad, suggesting their nanocrystalline and pure nature.

3.3. SEM-EDAX analysis

The surface morphology and chemical composition of pure HA and Cr-HA with various concentrations are shown in Figs. 3 and 4, respectively. In the case of bone fracture crystal, the size distribution of the bone material plays an important role.[25] Fig. 3(a), showing pure HA, reveals that the particles are agglomerates, consisting of small size and fine crystallites. Fig. 3(b,c,d,e,f) provides SEM images of the 0.5, 1.0, 1.5, 2.0, and 2.5 samples of Cr doped HA; these images indicate the morphology of the particles and the size of the particles. It was observed that, with the increase in the Cr^{3+} concentration in the HA lattice, an irregular shape of particles resulted. The EDS patterns of HA and Cr-HA show the elemental compositions of Ca, P, O, and Cr. The elemental composition of HA and Cr-HA is tabulated in Table 1. The obtained atomic ratios suggest that the samples are stoichiometric. The obtained Ca/P atomic ratio for

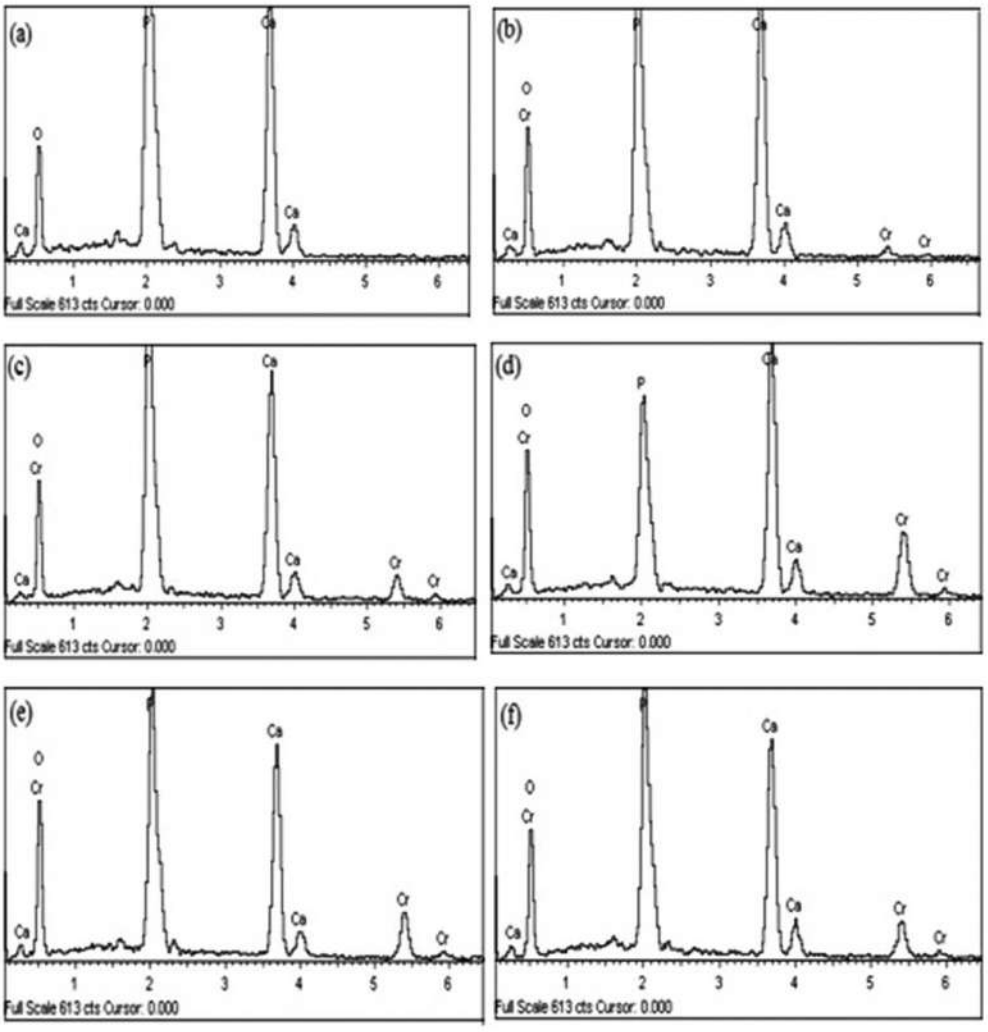

Fig. 4. EDS spectrum of (a) pure HA, (b) Cr-HA-1, (c) Cr-HA-2, (d) Cr-HA-3, (e) Cr-HA-4, and (f) Cr-HA-5.

Table 1. Elemental Composition of HA and Cr-HA Nanoparticles

Sample	Atomic % composition			
	Cr	Ca	P	O
HA	-	32.33	19.52	48.15
Cr-HA-1	0.94	26.15	17.47	55.38
Cr-HA-2	1.95	26.09	17.46	54.50
Cr-HA-3	2.27	23.12	15.93	58.68
Cr-HA-4	3.57	23.25	16.12	57.06
Cr-HA-5	4.48	22.90	16.20	56.42

pure nanocrystalline HA is 1.66, which is close to the standard value (Ca/P = 1.67). The Ca/P atomic ratios (1.50, 1.49, 1.45.1.44, and 1.41) for the Cr-HA samples are almost equal to the standard, as is shown in Table 1. It can be seen that there is a slight decrease in the Ca/P atomic ratio in the Cr-HA samples. The obtained results reveal the proper substitution of Ca with Cr metal ions during the synthesis process. The Ca/P atomic ratios between 1.33 - 1.55 could be very beneficial for the formation of new bone *in-vivo*.

3.4. TEM analysis

TEM analysis results of pure HA and Cr-HA calcined at 900ºC for 2 h are shown in Fig. 5. The results for pure HA shown in Fig. 5(a) indicate the slight agglomeration of particles with rod shape morphology; the size was found to be in a range of 100 nm in diameter with homogeneous microstructure. The representative samples of Cr-HA in Fig. 5(b) show the rod shape with slight agglomeration, which strongly confirms the crystallite size of the XRD and SEM analysis.

The enhancement in the formation of rod shape indicates that the amount of Cr^{3+} consists of replacement of Ca^{2+} ions in the HA crystal structure during the synthesis process, which can have an effect on the nucleation of particles and can lead to particle agglomeration. The inset of Fig. 5(a) and (b) shows the corresponding SAED patterns of the HA and Cr-HA5 samples. The presence of bright ring patterns confirms the polycrystalline nature of the Cr-nanoparticles.

3.5. In vitro biocompatibility study

To examine in detail the biocompatibility of HA and Cr-HA, it is suggested to use several cell-based assays in different cell lines with different incubation times and doses of nanoparticles. Using MTT assay, the pure HA and Cr-HA powder that was used in the compatibility study is examined to verify the cell viability and cytocompatibility behaviour of the Hela (Cervical cancer) cells and L929 (mouse fibroblast) cells for incubation times of 12 and 24 h at different concentrations from 10, 50, 100, 200, 400, and 800 µg/ml. The percentages of cell viability are shown in Fig. 6. The obtained results for the MTT assay reveal that as the concentration of the nanoparticles and the incubation time increase, these factors gradually decrease the cell viability. The Hela and L929 cells were highly compatible and metabolically active when they were in contact with the 10, 50, 100, 200, 400, 800 µg/ml sample concentrations. Previous reports are available on teh cytotoxicity effects of certain nanoparticles in the MTT assay and on the mechanism of the cytotoxicity due to nanoparticles.[26,27] It has been reported that when nanoparticles are present on the cell surface they affects the plasma membrane after a certain period of time and cause the breakdown of the cell wall of the cell.[28] Then, after the nanoparticles are removed from the cell surface and both the cells are stained with MTT, the MTT moves into the cells and passes into the mitochondria, where it is reduced to coloured formazan, an insoluble product because living cells decrease yellow tetrazolium salt to a purple dye. Then, these cells can be dissolved with isopropanol (an organic solvent) and the obtained formazan can be spectrophotometrically measured. The reduction of MTT is

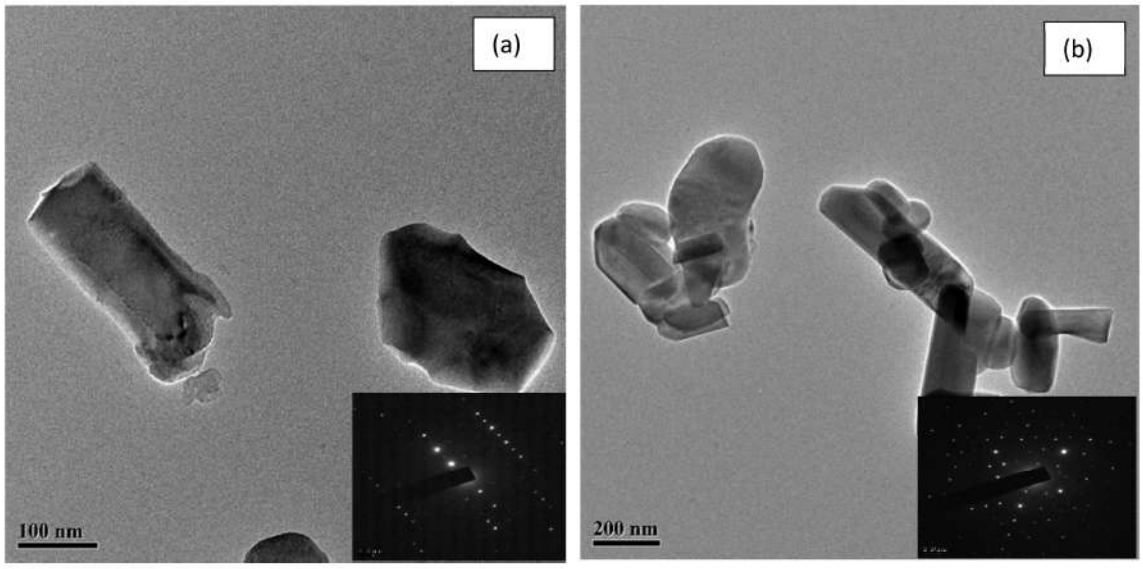

Fig. 5. TEM images of (a) HA and (b) Cr-HA-5. (Inset: corresponding SAED pattern).

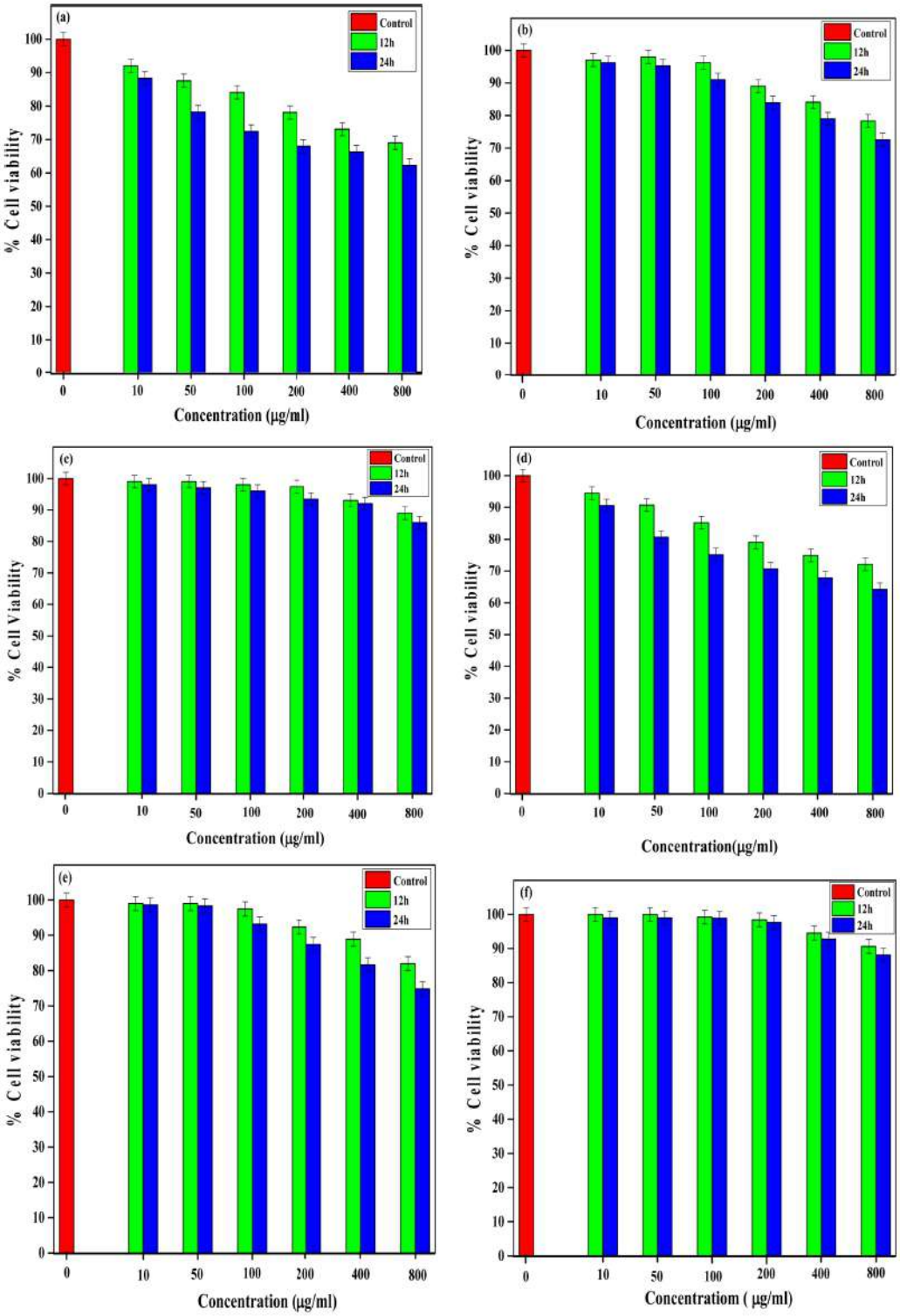

Fig. 6. Biocompatibility study on Hela cervical cell line. (a) pure HA, (b) Cr-HA1, (c) Cr-HA5. Biocompatibility study on L929 cell line (d) pure HA (e) Cr-HA1 (f) Cr-HA5 for 12 and 24 h.

only known to occur in metabolically active cells. A higher cell cytotoxicity is observed for the Hela cells as compared to that of the L929 cell lines. The cell viability values for the 800 µg/ml sample of pure HA or Hela cells are observed to be about 69 and 62%; for the Cr1-HA nanoparticles, these values are 78 and 73%, and the Cr5-HA nanoparticles on Hela cells are observed to have values of about 89 and 86% for 12 and 24 h, respectively.

The cell viability values for the 800 µg/ml samples of pure HA and L929 cells are observed to be about 73 and 65%; for

the Cr1-HA nanoparticles, these values are 82 and 75%, and for the Cr5-HA nanoparticles these values are about 91 and 88% for 12 and 24 h, respectively. The same nanoparticles show different levels of cell viability between cell lines; it is probable that this is due to differential cell vision effects (differential interactions with the same nanoparticles in different cells, known as "cell vision" effects), the surface properties of the cell types, and differences in the cell morphology Moreover, different cell types show different levels of metabolic activity.[29,30] From the observed results it is clear that a higher cytotoxicity is observed in the HA as compared to the Cr-HA nanoparticles. It is reported that HA is biocompatible with the L929 cells.[31] The obtained results reveal that the viability of the Hela and L929 cell lines is affected by the presence of Cr(III), suggesting that Cr-HA nanoparticles do not possess a toxic effect and are highly biocompatible. Cr doped HA nanoparticles can possibly be used for further in vivo applications.

3.6. In vitro Hemocompatibility

Hemocompatibility is essential characteristic for materials that are intended for use as implants or that are in direct contact with blood. A hemolysis assay was performed to study the effects of HA and Cr-HA on hemolytic activity and on the integrity of the RBC membrane. The hemolytic ratio was reported to be in three categories including < 2%, 2 - 5%, and > 5%; these shall be labelled as slightly non hemolytic, hemolytic, and hemolytic, respectively.[32] The obtained hemolytic results for pure HA and Cr-HA are shown in Fig. 7. The hemolytic ratio was found to progressively improve in a range from HA to HA samples doped with various concentrations of Cr. These results allow us to conclude that pure HA and Cr-HA1 have hemolytic ratios of 1.0 and 1.1%, which indicate that these materials are exceedingly hemocompatible and have hemolytic ratios less than 2%. On the other hand, the Cr-HA2, Cr-HA3, Cr-HA4, and Cr-HA5 samples of Cr doped HA have been found to have hemolytic ratios of 1.8, 2.7, 3.9, and 4.6%, respectively, which mean that this group is slightly toxic (haemolytic ratio in range of 2 - 5%) toward red blood cells. Therefore, the hemolytic ratio was observed to increase in a range from HA to Cr doped HA due to the increase in the combination of Cr doping. Due to the Cr doping, HA decreases in terms of its crystalline nature, which leads to a rise in the level of resorption. The released Cr ions may interact with RBC membranes and cause breakage; lastly, they can release hemoglobin (Hb) from erythrocytes.[33] The observed data for HA and Cr-HA are near to the reported limit (5%). Therefore, the observed data confirm that pure HA and Cr-HA show hemolytic ratios less than 5%; the data also reveal that the developed Cr-HA can be used for *in vivo* biomedical applications.

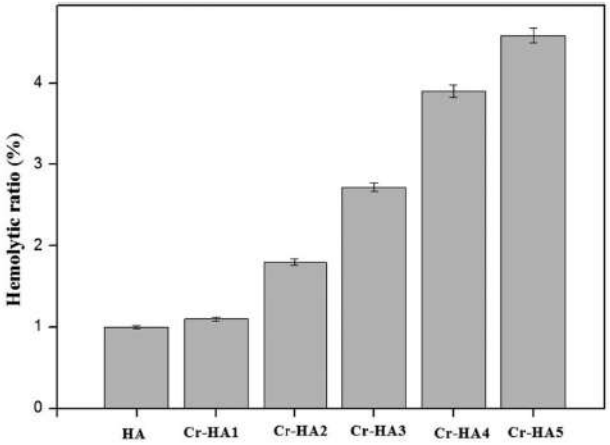

Fig. 7. *In vitro* hemocompatibility study of pure HA, Cr-HA1, Cr-HA2, Cr-HA3, Cr-HA4, and Cr-HA5.

4. Conclusions

In this present research work, we have successfully synthesized pure HA and Cr-HA (0.5, 1.0, 1.5, 2.0, and 2.5) by solution combustion method. The XRD analysis confirms the pure phase formation of Cr doped HA without any other secondary phases; it was concluded that the crystallite size and the crystallinity slowly decreased with moderately increased lattice parameters in a range from Cr-HA1 to Cr-HA5 due to the replacement of Ca^{2+} with Cr^{3+} ion in HA.

The SEM and TEM analysis confirmed a rod shaped surface morphology with good agglomeration of Cr-HA. The EDS spectra of HA and Cr-HA confirm the existence of Ca, P, and Cr elements and confirm that the Ca/P ratio is in a range of 1.41 - 1.66. *In vitro* hemocompatibility results reveal the very compatible nature of this material with RBC and HA; Cr-HA shows a hemolytic ratio of less than 5% and this confirms that these Cr-HA powders have good hemocompatible behaviour. *In vitro* cytotoxicity study was performed on Hela and L929 cell lines and the results indicated that both types of cells were highly cytocompatible up to a concentration of 800 µg/ml and for a duration of 24 - 48 h; this compatibility might be due to the release of Cr^{3+} ions from the Cr-HA powder. Therefore, these *in vitro* biological studies proved that Cr doped HA powders can be used as promising ceramic materials for biomedical applications.

REFERENCES

1. L. L. Hench, "Bioceramics," *J. Am. Ceram. Soc.*, **81** [7] 1705-28 (1998).
2. S. V. Dorozhkin, "A Detailed History of Calcium Orthophosphates from 1770s till 1950," *Mater. Sci. Eng., C*, **33** [6] 3085-110 (2013).
3. S. V. Dorozhkin and M. Epple, "Biological and Medical Significance of Calcium Phosphates," *Angew. Chem., Int. Ed.*, **41** [17] 3130-46 (2002).
4. H. Q. Cao, L. Zhang, H. Zheng, and Z. Wang, "Hydroxyapatite Nanocrystals for Biomedical Applications," *J. Phys. Chem. C*, **114** [43] 18352-57 (2010).
5. E. S. Ahn, N. J. Gleason, A. Nakahira, and J. Y. Ying, "Nanostructure Processing of Hydroxyapatite-Based Bioceramics," *Nano Lett.*, **1** [3] 149-53 (2001).

6. D. Tanaskovic, B. Jokic, G. Socol, A. Popescu, I. N. Mihailescu, R. Petrovic, and D. Janackovic, "Synthesis of Functionally Graded Bioactive Glass-Apatite Multistructures on Ti Substrates by Pulsed Laser Deposition," *Appl. Surf. Sci.*, **254** [4] 1279-82 (2007).
7. K. Hayashi, T. Mashima, and K. Uenoyama, "The Effect of Hydroxyapatite Coating on Bony Ingrowth into Grooved Titanium Implants," *Biomaterials,* **20** [2] 111-19 (1999).
8. H. F. Morris and S. Ocbi, "Hydroxyapatite-Coated Implants: A Case for Their Use," *J. Oral Maxillofac. Surg.,* **56** [11] 1303-13 (1998).
9. H. Zhou and J. Lee, "Nanoscale Hydroxyapatite Particles for Bone Tissue Engineering," *Acta Biomater.,* **7** [7] 2769-81 (2011).
10. C. J. Chung, R. T. Su, H. J. Chu, H. T. Chen, H. K. Tsou, and J. L. He, "Plasma Electrolytic Oxidation of Titanium and Improvement in Osseointegration," *J. Biomed. Mater. Res., Part B,* **101** [6] 1023-30 (2013).
11. Y. Tanaka, Y. Hirata, and R. Yoshinaka, "Synthesis and Characteristics of Ultrafine Hydroxyapatite Particles," *J. Ceram. Process. Res.*, **4** [4] 197-201 (2003).
12. I. Smiciklas, A. Onjia, J. Markovic, and S. Raicevic, "Comparison of Hydroxyapatite Sorption Properties towards Cadmium, Lead, Zinc and Strontium Ions," *Mater. Sci. Forum*, **494** 405-10 (2005).
13. R. Z. LeGeros, "Calcium Phosphate-Based Osteoinductive Materials," *Chem. Rev.*, **108** [11] 4742-53 (2008).
14. E. D. Berry and G. R. Siragusa, "Hydroxyapatite Adherence as a Means to Concentrate Bacteria," *Appl. Environ. Microbiol.,* **63** [10] 4069-74 (1997).
15. M. Niinomi, M. Nakai, and J. Hieda, "Development of New Metallic Alloys for Biomedical Applications," *Acta Biomater.*, **8** [11] 3888-903 (2012).
16. K. S. Oh, K. J. Kim, Y. K. Jeong, and Y. H. Choa, "Effect of Fabrication Processes on the Antimicrobial Properties of Silver Doped Nano-Sized Hap," *Key Eng. Mater.,* **240** 583-86 (2003).
17. M. Wakamura, K. Kandori, and T. ishikawa, "Surface Structure and Composition of Calcium Hydroxyapatites Substituted with Al(III), La(III) and Fe(III) Ions," *Colloids Surf., A,* **164** [2] 297-305 (2000).
18. B. Alemón, M. Flores, W. Ramírez, J. C. Huegel, and E. Broitman, "Tribocorrosion Behavior and Ions Release of CoCrMo Alloy Coated with a TiAlVCN/CN_x Multilayer in Simulated Body Fluid Plus Bovine Serum Albumin," *Tribol. Int.*, **81** 159-68 (2015).
19. W. Brodner, P. Bitzan, V. Meisinger, A. Kaider, F. Gottsauner-Wolf, and R. Kotz, "Elevated Serum Cobalt with Metal-on-Metal Articulating Surfaces," *J. Bone Jt. Surg., Br. Vol.,* **79** [2] 16-21 (1997).
20. P. Collery, Y. Maymard, T. Theophanides, L. Khassanova, and T. Collery, "Metal Ions in Biology," *J. John Libbey: New Barnet*, **10** 739-42 (2008).
21. S. A. Katz and H. Salem, "The Toxicology of Chromium with Respect to its Chemical Speciation: A Review," *J. Appl. Toxicol.,* **13** [3] 217-24 (1993).
22. G. Mabilleau, R. Filmon, P. K. Petrov, M. F. Baslé, A. Sabokbar, and D. Chappard, "Cobalt, Chromium and Nickel Affect Hydroxyapatite Crystal Growth *in vitro*," *Acta Biomater.,* **6** [4] 1555-60 (2010).
23. J. Devoya, A. Gehinb, S. Mullera, M. Melczera, A. Remya, G. Antoinea, and I. Sponnec, "Evaluation of Chromium in Red Blood Cells as an Indicator of Exposure to Hexavalent Chromium: An *in vitro* Study," *Toxicol. Lett.*, **255** 63-70 (2016).
24. H. M. Yadav, T. V. Kolekar, A. S. Barge, N. D. Thorat, S. D. Delekar, B. M. Kim, B. J. Kim, and J. S. Kim, "Enhanced Visible Light Photocatalytic Activity of Cr^{3+}-Doped Anatase TiO_2 Nanoparticles Synthesized by Sol–Gel Method," *J. Mater. Sci.: Mater. Electron.,* **27** [1] 526-34 (2016).
25. M. J. Phillips, J. A. Darr, Z. B. Luklinska, and I. Rehman, "Synthesis and Characterization of Nano-Biomaterials with Potential Osteological Applications," *J. Mater. Sci.: Mater. Med.,* **14** [10] 875-82 (2003).
26. T. Metanawin, T. Tang, R. Chen, D. Vernon, and X. Wang, "Cytotoxicity and Photocytotoxicity of Structure-Defined Water-Soluble C_{60}/Micelle Supramolecular Nanoparticles," *Nanotechnology,* **22** [23] 235-39 (2011).
27. H. Yin, P. S. Casey, M. J. McCall, and M. Fenech, "Effects of Surface Chemistry on Cytotoxicity, Genotoxicity, and the Generation of Reactive Oxygen Species Induced by ZnO Nanoparticles," *Langmuir,* **26** [19] 15399-408 (2010).
28. K. C. Barick, S. Singh, N. V. Jadhav, D. Bahadur, B. N. Pandey, and P. A. Hassan, "pH-Responsive Peptide Mimic Shell Cross-Linked Magnetic Nanocarriers for Combination Therapy," *Adv. Funct. Mater*, **22** [23] 4975-84 (2012).
29. D. A. Mbeh, R. Franaça, Y. Merhi, X. F. Zhang, T. Veres, E. Sacher, and L. Yahia, "*In vitro* Biocompatibility Assessment of Functionalized Magnetite Nanoparticles: Biological and Cytotoxicological Effects," *J. Biomed. Mater. Res., Part A,* **100** [6] 1637-46 (2012).
30. D. Richards and A. Ivanisevic, "Inorganic Material Coatings and Their Effect on Cytotoxicity," *Chem. Soc. Rev.*, **41** [6] 2052-60 (2012).
31. T. V. Kolekar, N. D. Thorat, H. M. Yadav, V. T. Magalad, M. A. Shinde, S. S. Bandgar, J. H. Kim, and G. L. Agawane, "Nanocrystalline Hydroxyapatite Doped with Aluminium: A Potential Carrier for Biomedical Applications," *Ceram. Int.,* **42** [4] 5304-11 (2016).
32. P. T. Kashmira, S. C. Kiran, S. T. Vrinda, and J. J. Mihir, "Pure and Zinc Doped Nano-Hydroxyapatite: Synthesis, Characterization, Antimicrobial and Hemolytic Studies," *J. Cryst. Growth.,* **401** 474-79 (2014).
33. M. Zhifang, B. Jing, W. Yichen, and J. Xiue, "Impact of Shape and Pore Size of Mesoporous Silica Nanoparticles on Serum Protein Adsorption and RBCs Hemolysis," *ACS. Appl. Mater. Interfaces,* **6** [4] 2431-38 (2014).